OPTICAL FIBER BASED LOW TEMPERATURE SENSORS

M K GHOSH*, P K DUTTA
S SANJIV and PIYUSH KUMAR
Department of Electrical Engineering
Indian Institute of Technology
Kharagpur 721302. India.

Abstract Design of optical fiber based low temperature sensors for application in cryogenic ranges is presented. The performance characteristics of the microbend sensors are quite satisfactory and there is scope for improvement by choosing suitable materials and configuration. The interferometric phase modulated sensor is highly sensitive and inconvenient for practical use in its conventional form. Immunity to EMI, intrinsic safety and small size are major attractions of the optical fiber based sensors.

Keywords: Thermometer, Optical Fiber Sensor, And Cryogenic Instrumentation.

INTRODUCTION

A few mechanical and electrical temperature sensors show sensitivity in a range that extends to the cryogenic temperature region [Rangan et al, 1997], e.g., liquid in glass thermometers (mercury – 38° to 630° C, organic liquids like mixtures of pentane and alcohol or toluene – 200° to 200° C), liquid filled thermometers (-35° to 500° C), vapour pressure thermometers (- 40° to 350° C), thermocouples (copper–constantan - 200° to 400° C, iron–constantan –200° to 700°C),resistance thermometers (platinum – 180° to 630° C, nickel – 60° to 150° C, thermistors – 100° to 300° C, semiconductors based – 270° to 180° C). Though optical pyrometers are very good for high temperature ranges, total radiation pyrometers can be used from – 50° to 2000° C. However, considering sensor size and applicability, span, linearity, accuracy and dynamic response, the thermometers used for cryogenic temperature measurement are: organic liquid in glass thermometers, thermocouples, resistance thermometers, thermistors and semiconductor sensors. Thin film platinum resistance thermometers find application in space. 'Cryo– tracker' [Haberbusch, 2001] developed by Sierra Lobo consists of a [Haberbusch, 2001] developed by Sierra Lobo consists of a series of polyamide layers (0.0254 mm) that insulate the temperature elements thermally from environment and electrically from each other, and provide mechanical protection. Rakes of temperature elements are made of stainless steel tubing, wire and phenolic insulators. It has a wide range (1.4 to 320 K).

Development of optical fiber based sensors (OFS) [Giallorenzi et al, 1982, Davis et al, 1987] has opened a new vista in sensor family that possess a number of unique characteristics. The OFS commonly used for temperature sensing are refractive index modulated (25° to 60° C), wavelength modulated (liquid crystal based 25° to 60° C, radiation pyrometer in the high range) and phase modulated (interferometric). In the present work development of a novel intensity modulated microbend OFS and investigation on suitability of an interferometric OFS in the cryogenic range are presented.

*Email: ghoshmk@yahoo.com

MICROBENDING LOSS

Mechanism

An optical fiber when subjected to microbending i.e., the radius of curvature of its bend is small compared with the fiber radius, coupling from propagating modes to radiation modes is induced resulting in loss of optical power. Total number of propagating modes is approximately

$$M = 0.5(\varphi / \varphi + 2)\, V^2 \quad \ldots \ldots \ldots \quad (1)$$

where $V = (2\pi / \lambda_{0)}\, a\, (n_1^2 - n_2^2)^{1/2} = \beta_0 a\, (NA)$, a= core radius, n_1 and n_2 are RI of core and cladding respectively, λ_0 is the wavelength of incident light in free space, β_0 is the propagation constant = $2\pi / \lambda_0$, NA is the numerical aperture = $(n_1^2 - n_2^2)^{1/2} = n_1 (2\,\Delta)^{1/2}$, if $\Delta=(n_1 - n_2) / n_1 << 1$.

For a step index fiber, $\varphi = \infty$, and $M \approx 0.5V^2$, for V >10

$$\ldots \quad (2)$$

For a parabolic index fiber, $\varphi = 2$, and $M \approx 0.25\, V^2$

$$\ldots \quad (3)$$

For a single mode fiber $V \leq 2.405$ and only the fundamental mode is propagated.

In the expression is for electromagnetic wave propagation, putting $k = \omega (\mu_0 \varepsilon_0)^{1/2} n$, the condition for cut off of the modes is $\beta / k = n_2$, where ω is the angular frequency, μ_0 , ε_0 are the permeability and permittivity

of free space. At very far off cut off frequency, i.e., $V \rightarrow \infty$, $\beta = n_1 k$. The electromagnetic energy of a guided mode is carried partially in the core and partially in the cladding. The cladding mode power constitutes the radiation loss. The power flowing in the core is due to the modes that are far off from its cut off frequency.
The relative amount of power flowing in core and cladding is determined by integrating the Poynting vector in the axial direction. Thus,

$$P_{core} = \tfrac{1}{2} \int_0^{2\pi} \int_0^a r (E_x H_y^* - E_y H_x^*) \, dr \, d\phi \quad \ldots (4)$$

$$P_{clad} = \tfrac{1}{2} \int_0^{2\pi} \int_a^{\infty} r (E_x H_y^* - E_Y H_x^*) \, dr \, d\phi \quad \ldots (5)$$

Noting that total power $P = P_{core} + P_{clad,}$ plot of P_{core} / P [Agarwal, 1993, Davis et al, 1987] signifies that near cut off frequency the power of the two lowest modes (HE_{11}, HE_{21}) is concentrated in the cladding (radiation mode) where as the higher modes still have a significant fraction of this power at cut off. If we assume an incoherent source to excite every fiber mode with the same amount of power, the total average core power can be approximated as

$$(P_{core} / P)_{total} = 1 - (P_{clad} / P)_{total} = 1 - 4 / 3 M^{-\frac{1}{2}} \quad \ldots (6)$$

Since $M \propto V^2$, power flow in the core increases as V increases. The number of degenerated modes, i.e., modes which have their β values within a specific limit of β_0 and $\beta_{m,}$ that take part in mode coupling is given by

$$m = \int_0^{rm} [\beta_0'^2 - \beta^2_m] r \, dr = \int_0^{rm} [n^2 (r) k_0^2 - \beta^2_m] \, r \, dr \quad \ldots (7)$$

$$\text{where } r_m = a[\{1 - (\beta_m / n_0 k_0)^2\} / 2\Delta]^{1/\varphi} \quad \ldots (8)$$

Usual microbending loss is associated with the random bends in the fiber (cabling or packaging losses) and core diameter fluctuations. The fundamental mode power is coupled to higher modes and then to the radiation mode causing attenuation of the propagating modes, more specifically of the fundamental mode. Microbending loss is also dependent on NA of the fiber [Davis et al, 1987], on the modal power distribution present within the fiber and the loss decreases at longer wavelengths.

Induced Microbending Loss
Induced microbending of an optical fiber is associated with forced coupling of power between modes; between the propagating and between propagating and radiation modes. The difference between any two longitudinal propagation constants is given by [Giallorenzi et al, 1982]

$$\delta\beta = \beta_{m+1} - \beta_m = [\varphi / \varphi + 2]^{\frac{1}{2}} (2\sqrt{\Delta} / a) [m / M]^{(\varphi - 2)/(\varphi + 2)} \quad \ldots (9)$$

For parabolic GRIN fiber $\varphi = 2$ and $\delta\beta = (2\Delta)^{\frac{1}{2}} / a \quad \ldots (10)$

For step index fiber $\varphi = \infty$ yields $\delta\beta = (2\Delta^{\frac{1}{2}}) m / aM \quad \ldots (11)$

The above signifies that in a parabolic GRIN fiber $\delta\beta$ is independent of m and all modes are equally spaced. Thus, for parabolic index fiber a critical distortion wavelength exists for optimum coupling between adjacent modes, e.g.

$$\lambda_c = 2a / (2\Delta)^{\frac{1}{2}} \quad \ldots (12)$$

However, no such critical wavelength exists for step index fiber, since the modes are not equally spaced. A comparison indicates that modes in a GRIN fiber are more confined to the core of the guide than those in a step index fiber.

Microbend OFS
For a multimode fiber, the ith mode has the electric field

$$E_i = E_0 \sin(\omega t - \beta_i z), \; i = 1,2,\ldots M \quad \ldots (13)$$

However, when microbending is induced, some propagating modes radiate into cladding mode. The coupling condition between any two modes or between the propagating mode (β_{core}) and the cladding mode (β_{clad}) is given by (for all fibers)

$$(\beta_{m+1} - \beta_m) \text{ or } (\beta_{core} - \beta_{clad}) = \pm 2\pi / L \quad \ldots (14)$$

where L is the spatial frequency or mechanical wavelength or pitch of the periodic distortion (Fig. 1).

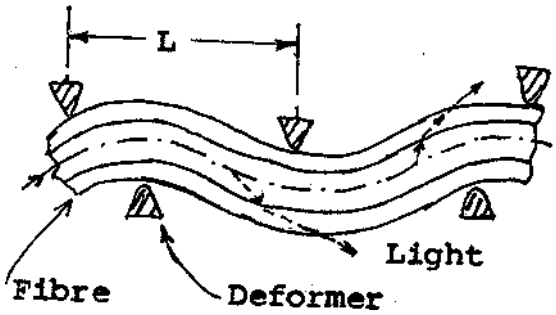

Fig.1 Coupling from core to cladding due to deformation of fiber.

In step index fibers the higher order modes are spaced further apart than lower order modes (eqn 11), and therefore coupling of higher order modes requires small L.The transduction element in a microbend OFS consists of a deforming device such as a pair of toothed or serrated plates that introduces small bends in a fiber (Fig. 2).

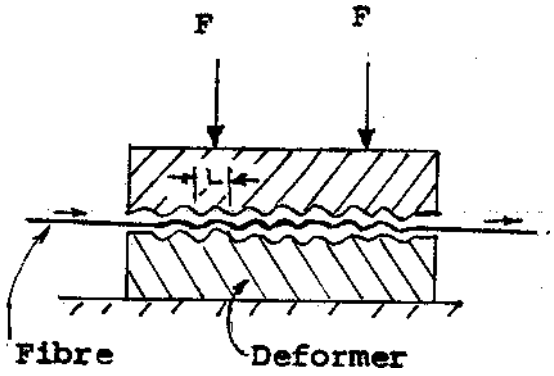

Fig. 2 Induced microbending in optical fiber

Because of the stiffness of the fiber, the bend radius changes slowly with more pressure (or force F) on the deformer blocks. The microbending loss obtained experimentally as a function of force (F) applied to the deformer with different angles of incidence of light [Davis et al, 1987] and for different V numbers in a GRIN fiber for uniform and steady state modal power distribution [Senior, 1996] show a good sensitivity and linearity of these types of force sensors.

Microbend OFS for Low Temperature Sensing

The underlying principle of design of this class of temperature sensor is based on implementing a suitable deformation mechanism that creates microbend as the temperature changes. Two ridged plates (deformers) sandwiching the optical fiber are clamped together such that at low temperature they contract towards the center causing sharper bends and greater loss of light. The complete system is presented in Fig. 3. In order to make the sensor sensitive to induced microbending loss only, cladding mode strippers are used before or after the sensor. Alternatively, a fiber with a lossy jacket (RI higher than that of cladding) is used.

Let the thermal coefficients of expansion be α_i, Young's Modulus of elasticity be E_i ,strain developed ε_i ,area on which the stress acts A_i , Force on the adjacent surface F_i , where i=0 for the optical fiber, 1 for the deformer material and 2 for the clamp material. Here $\alpha_2 >> \alpha_1 >> \alpha_0$ and n(T) is neglected.If the initial and final cryo temperatures are T_r and T respectively , for $T < T_r$, force on the deformer excerted by the clamp due to compression is

$$F_2 = E_2(\alpha_2 - \alpha_1)(T_r - T)A_2 \quad \ldots\ldots\ldots (15)$$

Similarly, the force on the optical fiber due to contraction of the contraction of the deformer is

$$F_1 = E_1(\alpha_1 - \alpha_0)(T_r - T)A_1 \quad \ldots\ldots\ldots (16)$$

However, with the configured deformer F_1 will not be effective as long as $\alpha_2 >> \alpha_1$. Hence the effective force on the optical fiber is essentially due to the clamp is only F_2 via deformer teeth. Between two adjacent teeth (A&B) of the deformer, separated by a distance L/2 (Fig. 4), the average force exerted on the fiber is

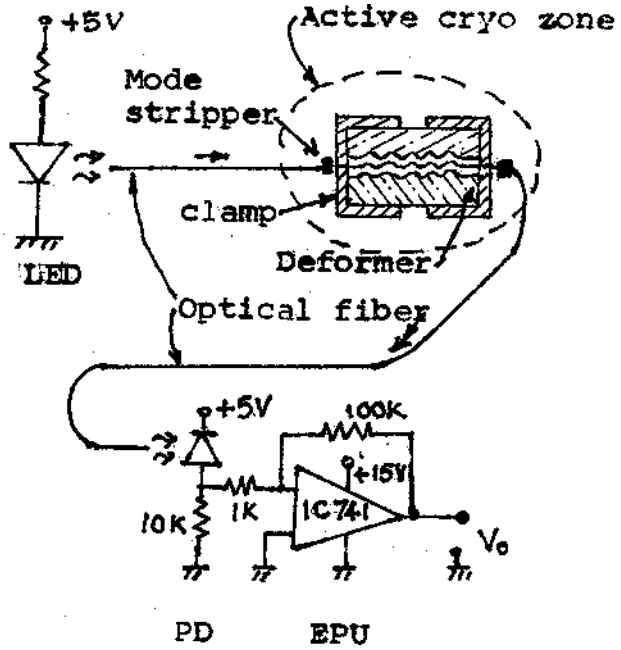

Fig. 3 Schematic of a microbend temperature sensor.

$$F_{0av} = F_2/n \quad \ldots\ldots\ldots (17)$$

Where n = no. of teeth in the deformer pair.

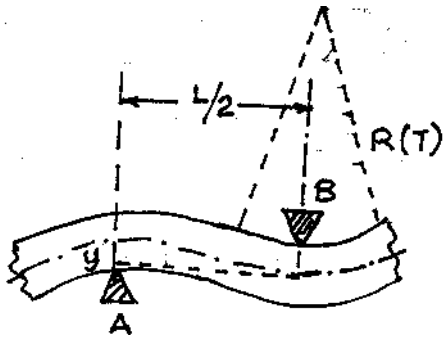

Fig. 4 Radius of curvature for a single segment.

The total length of the fiber sandwiched between the deformers is

$$L_0 = (n-1)L/2 \quad \ldots\ldots\ldots (18)$$

Due to the force on the fiber single segment, strain developed is

$$\varepsilon_0 = \{ [(L/2)^2 + (y)^2]^{1/2} - L/2 \}/ (L/2) \quad \ldots.(19)$$

where y = y(T) = displacement along the deformer teeth axis.

Force along the fiber axis is

$$F_0 = \varepsilon_0 . E_0 . A_0 \quad \ldots\ldots\ldots (20)$$

Force per tooth along the tooth axis is

$(F_0 \cos\theta)/2$ … … … (21)

where $\theta = \cos^{-1}(2y/L)$

Hence we have

$(F_0 \cos\theta)/2 = F_{0av} = E_2(\alpha_2 - \alpha_1)(T_r - T)A_2/n$ …. (22)

Combining equations (19),(20) and (22), we get

$$\{\{ [(L/2)^2 + (y)^2]^{1/2} - L/2 \}/ (L/2) \} \cos\theta =$$

$$2 E_2(\alpha_2 - \alpha_1)(T_r - T)A_2/nE_0A_0$$

or $\cos\theta [1/\sin\theta - 1] = c(T)$;or

$c(T) \tan\theta + \sin\theta = 1$ …. …. …. (23)

where c(T) is a temperature dependent constant.
Newton Raphson method was used to determine the value of θ at various temperatures.
As $y(T) = (L/2)\cot\theta$ (T) the radius of curvature can be determined .

$R(T) = [(L/2)^2 + (y(T))^2] / (2 y(T))$ … …. ….(24)

From Gloge equation [Agarwal ,1993] effective modes available after microbending

$$M_{eff} = M_\infty [1 - \{ (\varphi +2) / 2\varphi \Delta \}[2a/R(T) + \{3/2n_2kR(T)\}^{2/3}]]…(25)$$

where ,$M_\infty = \Delta \{ \varphi /(\varphi + 2) \}(n_1ka)^2$ and
$k = 2\pi / \lambda$

Putting eqn (25) in eqn (6)

$(P_{core}(T) / P)_{total} = 1 - 4/3 [M_{eff}]^{-1/2}$ … … … (26)

If the resistance of the photodiode in reverse bias is S when the optical power P_{core} falls on it ,

$S \propto \{ 1 - 4/3 [M_{eff}]^{-1/2} \} P_{total}$ … …. …. …(27)

The detector current $i \propto 1/S$. By using a series resistance $r \cong 10K\ \Omega$, the output of the amplifier of gain A_0 is

$V_0 = A_0 i r$ … … … …(28)

The plot of M_{eff} vs Temperature is given in Fig 5. It gives a theoretical assessment of the characteristics of the microbend optical fiber temperature sensor.

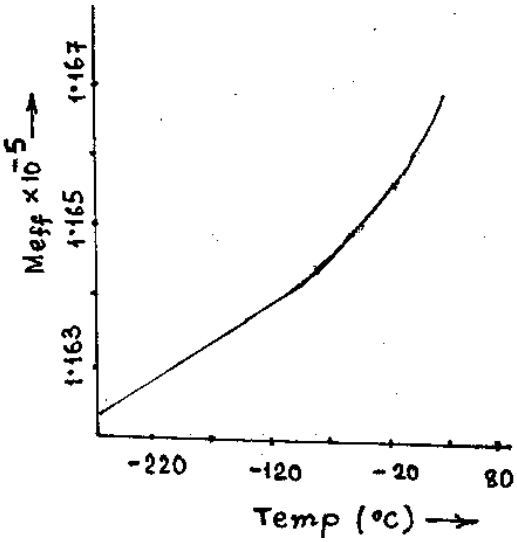

Fig. 5 Theoretical no. of effective modes.

TEST RESULTS

Experiments were performed with the following component specifications:

- **Optical fiber**: Plastic multimode step index
  $a_0 = 200\ \mu$ m
  $\alpha_0 = 1.54\ \mu$ m/m-K
  $E_0 = 4.8$ GPa
- **Clamp:** Teflon
  $\alpha_2 = 86\ \mu$ m/m-K
  $E_2 = 0.69$ GPa
- **Deformer:** Copper
  $\alpha_1 = 17\ \mu$ m/m-K
  $E_1 = 113$ GPa
- **LED:** Motorola, $\lambda = 780$ nm
- **Photodiode:** Motorola, IR (780 nm)

Cryostat temperature was varied from 140K to 220K and compared with a copper- constantan thermocouple. Results of both increasing and decreasing temperature are shown in Fig 6.

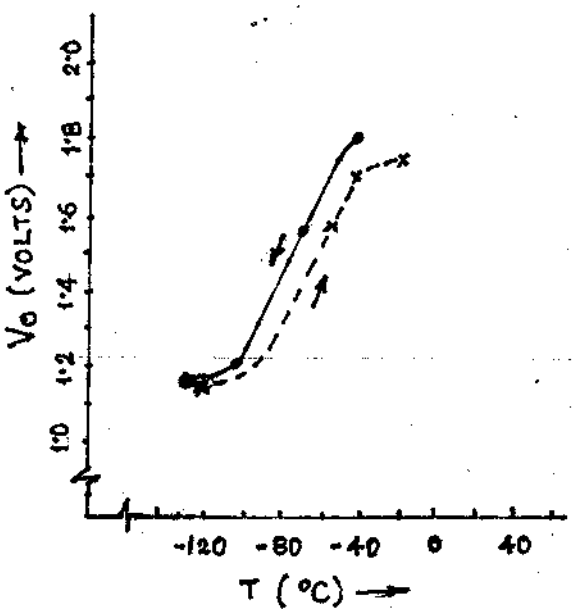

Fig. 6 Sensor response.

INTERFFEROMETRIC CRYOGENIC TEMPERATURE SENSOR

In an optical fiber, a temperature change ($\Delta\theta$) induces a change in its physical length (ΔL), a change in refractive index (Δn) and consequently a change in dispersion ($\Delta\tau$). The net effect is an induced phase shift ($\Delta\phi$) in the light propagating in the fiber. The effect of dispersion (τ) or pulse broadening on phase shift in the present sensor is negligible, as because (i) the predominant component (material dispersion) has comparatively little influence on phase shift, (ii) dispersion is length dependent (ps/nm/km) and $\Delta\tau$ is small, (iii) it can be reduced by choice of λ_g (guide wave length), and the sensor configuration (interferometer at the output stage) is such that it cancels the effects of dispersion. Thus, the dominant phase shift can be expressed as

$$\Delta\phi / \Delta\theta = 2\pi / \lambda_g [\, n \Delta L / \Delta\theta + L \Delta n / \Delta\theta \,] \quad \ldots \quad (29)$$

The value of thermal coefficient (α_0) and the temperature dependence of the RI ($n(\theta)$) vary greatly for multicomponent glasses. However, for fused silica the dominant effect is due to index change. The schematic diagram of the sensor is given in Fig 7.As expected the sensor was too sensitive to temperature fluctuation and hence unsuitable for continuous measurement of low temperature.

CONCLUSIONS

Out of two optical fiber based low temperature sensors developed and discussed in the paper, the interferometric sensor was found to be too sensitive for any practical application. However, it can be used for detection of very small temperature variation in scientific measurements. The microbend sensor has good static and dynamic characteristics. The range of operation depends on the fiber used, the materials and volume of the deformers and the configuration of the transduction element. The paper presents a version that operates in the range of 100 to 200 K. The experimental values were slightly differed from the theoretical values. One of the reasons for the difference may be coupling between the fundamental mode and the whispering gallery mode, which is formed from the light leaving the fundamental mode due to pure bending loss. More accurate methods used for solving such problems, such as, perturbation methods, are rather tedious. Experimental calibration is much easier. The sensor finds application in magnetic field use and in hazardous environment. It has a small size, and is capable of sensing and transmitting measured signal without additional circuitry. The current flowing in

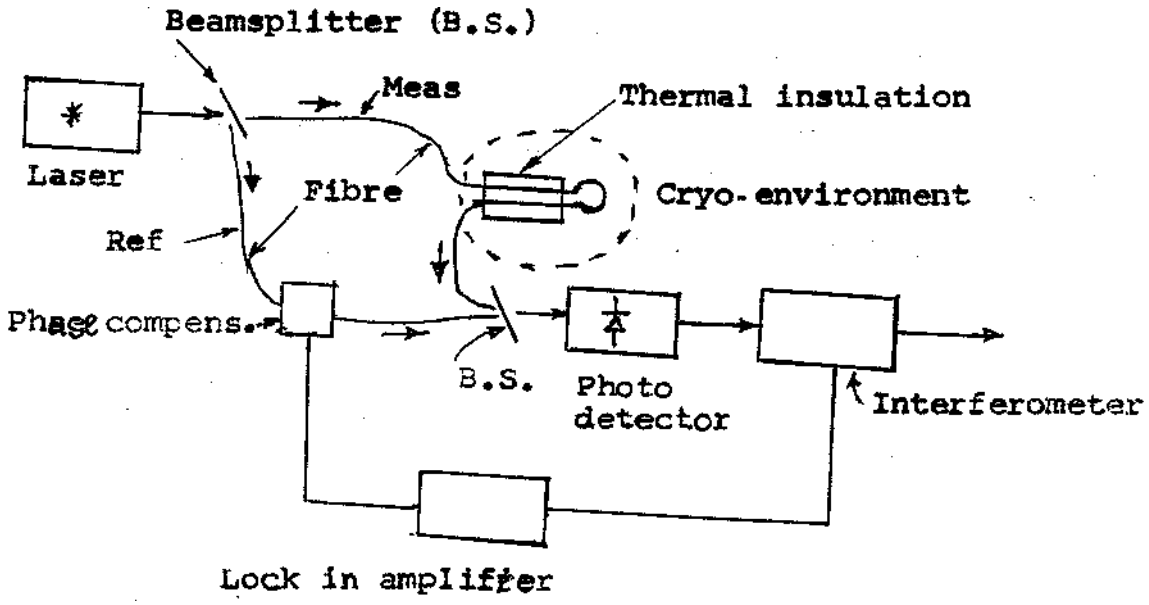

Fig. 7 Schematic of a phase modulated temperature sensor

electrical sensors may disturb the measuring environment to some degree, but these sensors are free from such problems.

ACKNOWLEDGEMENT

The authors gratefully acknowledge the help rendered by Prof.S.Pattnayak, Cryogenic Engineering Center, IIT Kharagpur in conducting the experiments.

REFERENCES

Agarwal, D.P., "*Fibre Optic Communication*", Wheeler Publishing, New Delhi, pp 124 to 143 (1993).

Cheo, P. K., "*Fiber Optics and Optoelectronics*", Prentice Hall, NJ, pp 66 to 71, 95 to 99 (1990)

Davis, C.M. et al, "*Fiber Optic Sensor Technology Handbook*", Dynamic Systems, Inc., Virginia, pp 2-7 to 2-10, 5-9 to 5-11 (1987).

Giallorenzi, T.G. et al, "Optical Fiber Sensor Technology", IEEE Journal of Quantum Elrctronics, Vol QE-18, No 4, pp 626 to 665 (April 1982).

Haberbusch, M.S., "Measuring Temperature and Liquid Level in Cryogenic Fluids", Sensors, Sierra Lobo Inc., Ohio, pp 1 to 5 (August 2001).

Rangan, C.S. Sarma, G.R., and Mani, V.S.V., "*Instrumentation Devices & Systems*", TMH Pub. Co., New Delhi, pp 186 to 187 (1997).

Senior, J.M., "*Optical Fiber Communications – Principles and Practice* ", PHI, New Delhi, pp 193 to 194 (1996).